J. Plasma Physics (1997), *vol.* 58, *part* 4, *pp.* 665–690. Printed in the United Kingdom

© 1997 Cambridge University Press

Alfvén-wave filamentation

S. CHAMPEAUX, T. PASSOT and P. L. SULEM

CNRS UMR 6529, Observatoire de la Côte d'Azur, BP 4229, 06304 Nice Cedex 4, France

(Received 14 October 1996 and in revised form 30 December 1996)

Transverse focusing or filamentation of weakly nonlinear Alfvén waves propagating in a dispersive medium is studied using an amplitude-equation formalism. Special attention is devoted to the small-β regime, where kinetic effects are weak and Alfvén-wave trains are unstable to convective filamentation. It is shown that, according to their initial duration, focusing wave packets can collapse in a finite distance or, conversely, the focusing can be arrested by the development of magnetosonic waves, which in both cases may lead to the formation of sharp acoustic fronts. This effect, which dominates the usual longitudinal steepening, provides an efficient mechanism to heat the plasma without requiring large-amplitude waves. It can significantly contribute to the acceleration of the solar wind.

1. Introduction

Alfvén waves play an important role in the dynamics of space plasmas, which are often permeated by a large-scale magnetic field (Belcher *et al.* 1969; Belcher and Davis 1971; Tu and Marsch 1995). For fully ionized media, the dissipation is weak (the ambipolar diffusion due to ion–neutral friction being negligible), but the dispersion is significant because of the Hall term arising in the generalized Ohm's law. In this paper, we investigate the transverse focusing or filamentation of Alfvén waves, a three-dimensional process, which is shown to yield a rapid steepening of magnetosonic waves and can thus significantly contribute to heating phenomena of the ambient medium, such as the solar wind or the interstellar medium. Other phenomena, such as decay instabilities (Viñas and Goldstein 1991*a*, *b*), which arise when the ratio $\beta^{1/2}$ of the sonic to Alfvén-wave velocities is smaller than unity, will not be considered here.

When, as in molecular clouds or at the base of the solar corona, the parameter β is sufficiently small, kinetic effects that can otherwise significantly affect the dynamics (Mjølhus and Wyller 1986, 1988; Mjølhus *et al.* 1989; Spangler 1989), are relatively weak, and the system can be accurately described in the framework of the dispersive MHD equations

$$\partial_t \rho + \boldsymbol{\nabla}\cdot(\rho\mathbf{u}) = 0, \tag{1.1}$$

$$\rho(\partial_t \mathbf{u} + \mathbf{u}\cdot\boldsymbol{\nabla}\mathbf{u}) = -\frac{\beta}{\gamma}\boldsymbol{\nabla}\rho^{\gamma} + (\boldsymbol{\nabla}\wedge\mathbf{b})\wedge\mathbf{b}, \tag{1.2}$$

$$\partial_t \mathbf{b} - \boldsymbol{\nabla}\wedge(\mathbf{u}\wedge\mathbf{b}) = -\frac{1}{R_i}\boldsymbol{\nabla}\wedge\left[\frac{1}{\rho}(\boldsymbol{\nabla}\wedge\mathbf{b})\wedge\mathbf{b}\right], \tag{1.3}$$

$$\boldsymbol{\nabla}\cdot\mathbf{b} = 0, \tag{1.4}$$

https://doi.org/10.1017/S0022377897006119 Published online by Cambridge University Press

where R_i is the non-dimensional gyromagnetic frequency of the ions and γ is the polytropic gas constant.

When the Alfvén waves are considered in the long-wavelength limit, their dynamics is often addressed in the framework of the derivative nonlinear Schrödinger (DNLS) equation (Rogister 1971; Mio *et al.* 1975; Mjølhus 1976), which requires very slow modulations in the transverse directions (Mjølhus and Wyller 1986, 1988). In Passot *et al.* (1994), the absolute filamentation process was studied in the limit of small carrier wavenumber, using amplitude equations derived from generalized three-dimensional DNLS equations that include the coupling to magnetosonic waves (Passot and Sulem 1993). Here, we obtain amplitude equations from the primitive MHD equations (1.1)–(1.4), and pay particular attention to the quasistationary convective instability that arises for small β. In Sec. 2, the relevant modulation equations are presented (leaving the details of the derivation for the appendix). It is noticeable that the anisotropic character of the problem affects the diffraction of the Alfvén wave, leading to equations different from those given in Zakharov and Rubenchik (1972) and Zakharov and Schulman (1991). Section 3 discusses the importance of filamentation compared with longitudinal steepening. Section 4 analyses the effect of a small deviation from purely transverse absolute and purely static convective instabilities. Section 5 addresses the nonlinear dynamics of a wave packet subject to filamentation, and the possible arrest of collapse due to the development of magnetosonic waves, which in both cases may lead to the formation of sharp fronts. In the conclusions (Sec. 6), possible applications of these phenomena to the solar wind are briefly discussed.

2. Modulation of dispersive Alfvén waves

The modulation analysis of a small-amplitude quasimonochromatic Alfvén-wave train propagating along an ambient magnetic field, whose modulus is taken as unity, is conveniently performed by introducing the slow variables $X = \epsilon^{1/2}x$, $Y = \epsilon^{1/2}y$, $Z = \epsilon^{1/2}z$ and $T = \epsilon^{1/2}t$, and expanding:

$$\rho = 1 + \epsilon(\rho_1 + \epsilon^{1/2}\rho_{3/2} + \ldots), \tag{2.1}$$

$$u_x = \epsilon(u_{x_1} + \epsilon^{1/2}u_{x_{3/2}} + \ldots) \tag{2.2}$$

$$b_x = 1 + \epsilon(b_{x_1} + \epsilon^{1/2}b_{x_{3/2}} + \ldots), \tag{2.3}$$

$$u_y = \epsilon^{1/2}(u_{y_{1/2}} + \epsilon^{1/2}u_{y_1} + \ldots), \tag{2.4}$$

$$u_z = \epsilon^{1/2}(u_{z_{1/2}} + \epsilon^{1/2}u_{z_1} + \ldots), \tag{2.5}$$

$$b_y = \epsilon^{1/2}(b_{y_{1/2}} + \epsilon^{1/2}b_{y_1} + \ldots), \tag{2.6}$$

$$b_z = \epsilon^{1/2}(b_{z_{1/2}} + \epsilon^{1/2}b_{z_1} + \ldots), \tag{2.7}$$

where the different magnitudes of the transverse and longitudinal components select the Alfvén-wave eigenmode.

At leading order, one gets the linear equations for strictly parallel propagation:

https://doi.org/10.1017/S0022377897006119 Published online by Cambridge University Press

$$\partial_t u_{y1/2} - \partial_x b_{y1/2} = 0, \tag{2.8}$$

$$\partial_t u_{z1/2} - \partial_x b_{z1/2} = 0, \tag{2.9}$$

$$\partial_t b_{y1/2} - \partial_x u_{y1/2} - \frac{1}{R_i}\partial_{xx} b_{z1/2} = 0, \tag{2.10}$$

$$\partial_t b_{z1/2} - \partial_x u_{z1/2} + \frac{1}{R_i}\partial_{xx} b_{y1/2} = 0. \tag{2.11}$$

It is easily checked that harmonic solutions of the form

$$b_{y1/2} = B_{y1/2}\, e^{i(kx-\omega t)} + \text{c.c.}, \tag{2.12}$$

$$b_{z1/2} = B_{z1/2}\, e^{i(kx-\omega t)} + \text{c.c.}, \tag{2.13}$$

satisfy $B_{y1/2} = i\zeta B_{z1/2}$, with $\zeta = -1$ or $\zeta = 1$ for right- or left-hand circularly polarized waves respectively. This contrasts with the non-dispersive limit, where arbitrary elliptical polarized solutions are possible (Hoshino 1988). The dispersion relation for longitudinal propagation, which can be viewed as the restriction of the dispersion relation

$$D(-i\Omega, ik_x, ik_y, ik_z) = 0 \tag{2.14}$$

of the full MHD equations to a wave vector with components $k_x = k$ and $k_y = k_z = 0$ and to the associated frequency ω (assumed positive), reads

$$\left(\frac{\omega}{k}\right)^2 = 1 - \frac{\omega}{R_i} \tag{2.15}$$

in the case of a left-hand polarized Alfvén wave, for which $b_y + ib_z \propto e^{i(kx-\omega t)}$, and

$$\left(\frac{\omega}{k}\right)^2 = 1 + \frac{\omega}{R_i} \tag{2.16}$$

for a right-hand polarized Alfvén wave obeying $b_y - ib_z \propto e^{i(kx-\omega t)}$. The variation of ω/R_i with k/R_i is displayed for both polarizations in Fig. 1(*a*), where, assuming that the wave propagates in the positive direction, we take $k > 0$. Furthermore, since the validity of the MHD description requires that $|\omega| < R_i$, the wavenumbers of right-hand polarized waves cannot exceed $R_i/\sqrt{2}$, while arbitrarily large values are possible in the case of left-hand polarization. Other ranges of frequencies, like that associated with electron-cyclotron waves, are addressed by Shukla and Stenflo (1986) and Stenflo and Shukla (1988).

Writing

$$b_{1/2} = b_{y1/2} + i\zeta b_{z1/2} = B_{1/2}\, e^{i(kx-\omega t)}, \tag{2.17}$$

$$u_{1/2} = u_{y1/2} + i\zeta u_{z1/2} = U_{1/2}\, e^{i(kx-\omega t)}, \tag{2.18}$$

where $\zeta = 1$ (left-hand polarization) or $\zeta = -1$ (right-hand polarization), we have

$$U_{1/2} = -\frac{k}{\omega} B_{1/2}. \tag{2.19}$$

https://doi.org/10.1017/S0022377897006119 Published online by Cambridge University Press

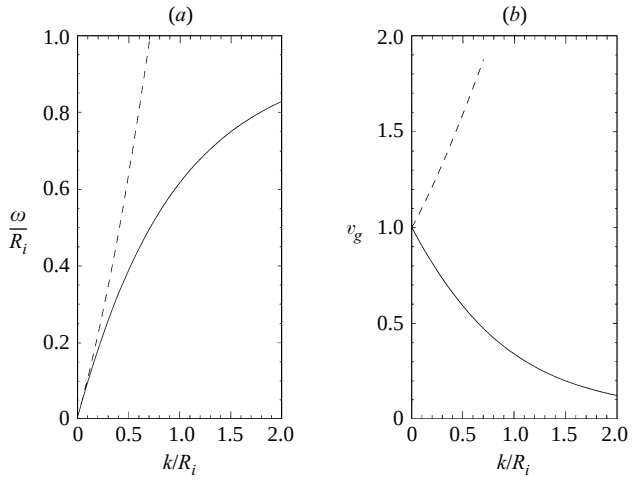


Figure 1. Variation with the wavenumber k/R_i, of the frequency ω/R_i (a) and the group velocity $v_g = \omega'$ (b), for left-hand polarized (solid lines) and right-hand polarized (dashed lines) Alfvén waves.

At order ϵ, the equations for the density and for the longitudinal components of the velocity and magnetic field read (writing $\partial_\perp = \partial_y + i\zeta\partial_z$)

$$\partial_t \rho_1 + \partial_x u_{x1} = -\tfrac{1}{2}(\partial_\perp^* u_{1/2} + \partial_\perp u_{1/2}^*), \tag{2.20}$$

$$\partial_t u_{x1} + \beta\partial_z \rho_1 = 0, \tag{2.21}$$

$$\partial_t b_{x1} = -\tfrac{1}{2}(\partial_\perp^* u_{1/2} + \partial_\perp u_{1/2}^*) + \zeta\frac{i}{2R_i}\partial_x(\partial_\perp^* b_{1/2} - \partial_\perp b_{1/2}^*), \tag{2.22}$$

$$\partial_x b_{x1} = -\tfrac{1}{2}(\partial_\perp^* b_{1/2} + \partial_\perp b_{1/2}^*). \tag{2.23}$$

They are solved as

$$\rho_1 = \tilde{\rho}_1 e^{i(kx-\omega t)} + \text{c.c.} + \bar{\rho}_1, \tag{2.24}$$

$$u_{x1} = \tilde{u}_{x1} e^{i(kx-\omega t)} + \text{c.c.} + \bar{u}_{x1}, \tag{2.25}$$

$$b_{x1} = \tilde{b}_{x1} e^{i(kx-\omega t)} + \text{c.c.} + \bar{b}_{x1}, \tag{2.26}$$

where overbars indicate non-oscillating contributions, which appear to be stirred at the next order of the expansion. The amplitudes of the oscillating parts are given by

$$\tilde{u}_{x1} = \frac{\beta k}{\omega}\tilde{\rho}_1, \tag{2.27}$$

$$\tilde{\rho}_1 = -\frac{ik}{2(\beta k^2 - \omega^2)}\partial_\perp^* B_{1/2}, \tag{2.28}$$

$$\tilde{b}_{x1} = \frac{i}{2k}\partial_\perp^* B_{1/2}. \tag{2.29}$$

The divergence for $\omega/k = \beta^{1/2}$ of the coefficient entering the definition of $\tilde{\rho}_1$ corresponds to the coincidence of the phase velocities of the Alfvén and magnetosonic waves. In the long-wavelength limit, where, to leading order, $|\omega| = |k|$, this resonance can only occur for $\beta = 1$. It was noticed in the framework

https://doi.org/10.1017/S0022377897006119 Published online by Cambridge University Press

of the long-wavelength reductive perturbation expansion of the dispersive MHD equations that, for β close to 1, the derivative nonlinear Schrödinger (DNLS) equation becomes invalid, and should be replaced by the TDNLS equations (T for 'triple'), considered in Hada (1993) and Webb *et al.* (1995), or by the uniform description given in Passot and Sulem (1995). The neighbourhood of this resonance is not amenable to an envelope description. Indeed, the (non-dispersive) small-scale sonic waves are in this case no longer slaved to the Alfvén wave. All the harmonics are thus resonant, which reflects the formation of weak shocks. This observation may question the relevance of the modulational stability analysis of the TDNLS equations performed in Hada (1993). Furthermore, kinetic effects are important in this case, and their consideration may prevent the resonance (Medvedev and Diamond 1995). The resulting dynamics is addressed in Galinsky *et al.* (1996) and Medvedev and Diamond (1996).

The details of the multiple-scale analysis describing the modulation of the Alfvén-wave amplitude and the dynamics of the mean fields introduced in (2.24)–(2.26) are given in the appendix. In order to get a closed system of equations without explicitly introducing a slower time scale or a longer length scale, it appears necessary to include subdominant corrections by defining $B = B_{1/2} + \epsilon^{1/2} B_1$, $\bar{\rho} = \bar{\rho}_1 + \epsilon^{1/2} \bar{\rho}_{3/2}$, $\bar{b}_{x_1} + \epsilon^{1/2} b_{x_{3/2}}$, $\bar{u}_x = \bar{u}_{x_1} + \epsilon^{1/2} \bar{u}_{x_{3/2}}$ and $\delta = \bar{\rho} - \bar{b}_x$. The resulting system reads

$$
\begin{aligned}
& i(\partial_T B + v_g \partial_X B) + \epsilon^{1/2} \alpha \Delta_\perp B \\
& \quad + \epsilon^{1/2} \frac{\omega}{k^2 + \omega^2} \left(\frac{\omega^2}{k^2} \partial_{XX} B + \frac{k^2}{\omega^2} \partial_{TT} B + \frac{2k}{\omega} \partial_{XT} B \right) \\
& \quad - \epsilon^{1/2} k v_g \left(\frac{1}{v_g} \bar{u}_x + \frac{k^2}{2\omega^2} \bar{b}_x - \frac{1}{2} \delta \right) B = 0, \qquad (2.30)
\end{aligned}
$$

$$
\partial_T \delta + \partial_X \bar{u}_x = 0, \qquad (2.31)
$$

$$
\partial_T \bar{u}_x + \beta \partial_X (\delta + \bar{b}_x) + \partial_X \frac{|B|^2}{2} = -i \frac{\alpha}{v_g} \epsilon^{1/2} (B \Delta_\perp B^* - B^* \Delta_\perp B), \qquad (2.32)
$$

$$
\partial_{TT} \bar{b}_x - \partial_{XX} \bar{b}_x - \Delta_\perp \left[\beta \delta + (\beta + 1) \bar{b}_x + \frac{k^2}{2\omega^2} |B|^2 \right] = 0. \qquad (2.33)
$$

In the above equations,

$$
v_g = \omega' = \frac{2\omega^3}{k(k^2 + \omega^2)} \qquad (2.34)
$$

is the group velocity of the Alfvén wave. Its variation with k for right- and left-hand polarizations is shown in Fig. 1(*b*). Furthermore, as expected,

$$
\alpha = \frac{k\omega}{k^2 + \omega^2} \left[\frac{\omega^2}{2k^3} - \frac{\beta k}{2(\beta k^2 - \omega^2)} \right] \qquad (2.35)
$$

identifies with $\frac{1}{2}\partial^2\Omega/\partial k_y^2$ or $\frac{1}{2}\partial^2\Omega/\partial k_z^2$, evaluated for $\Omega = \omega$, $k_x = k$ and $k_y = k_z = 0$.

The system (2.30)–(2.33) can be viewed as an initial-value problem either in time, in the context of the so-called absolute modulational instability (Kuo *et*

https://doi.org/10.1017/S0022377897006119 Published online by Cambridge University Press

al. 1988*a*) or in space, for the convective modulational instability (Kuo *et al.* 1988*b*). Using the facts that, to leading order, $\partial_T B + v_g \partial_X B = 0$, and that

$$\omega'' = 2\frac{\omega}{k^2+\omega^2}\left(\frac{\omega^2}{k^2}+\frac{k^2}{\omega^2}v_g^2-\frac{2k}{\omega}v_g\right),$$

the longitudinal and temporal dispersive terms arising in (2.30) can be rewritten in the usual form $\frac{1}{2}\omega''\partial_{XX}B$ for the absolute regime and $(\omega''/2v_g^2)\partial_{TT}B$ for the convective one. Furthermore, the term $-i\alpha\epsilon^{1/2}(B\Delta_\perp B^* - B^*\Delta_\perp B)$ in (2.32) is usefully replaced by $(\partial_T + v_g\partial_X)|B|^2 + \mathscr{D}$, with

$$\mathscr{D} \equiv -\tfrac{1}{2}i\omega''(B^*\partial_{XX}B - B\partial_{XX}B^*) = -\frac{i\omega''}{2v_g^2}(B^*\partial_{TT}B - B\partial_{TT}B^*).$$

Since it is only relevant when the transverse derivatives dominate the longitudinal (quasitransverse absolute dynamics) or the temporal ones (quasistatic convective dynamics), $\mathscr{D}$ is always negligible in the above expression, leading to the ponderomotive force given in Shukla *et al.* (1988).

3. When is filamentation relevant?

As is well known, (2.30) indicates that, to leading order, an Alfvén-wave packet is transported at the group velocity. To eliminate this trivial effect, in the absolute regime, the equations are written in a reference frame moving with the Alfvén-wave group velocity, by defining $\xi = X - v_g T$. A slower time scale $\tau = \epsilon^{1/2}T$, typical of the envelope dynamics, is then introduced. In the convective regime, the origin of time is taken to be space-dependent by defining $\tau = T - X/v_g$, and a longer length scale $\xi = \epsilon^{1/2}X$ is introduced. It follows that magnetosonic waves evolve on a time scale (absolute regime) or a length scale (convective regime) shorter by a factor of $\epsilon^{1/2}$ than the Alfvén-wave envelope.

3.1. Longitudinal modulational instability

In the case of purely longitudinal modulation, the limit $\epsilon \to 0$ is uniform. In this limit, $b_x = 0$ and the fields u_x and δ are slaved to the Alfvén-wave intensity. The modulation is thus governed by the canonical Schrödinger equation, which reads

$$i\partial_\tau B + \frac{\omega''}{2}\partial_{\xi\xi}B + \frac{kv_g}{4(\beta - v_g^2)}|B|^2 B = 0 \tag{3.1}$$

in the absolute regime, or

$$i\partial_\xi B + \frac{\omega''}{2v_g^3}\partial_{\tau\tau}B + \frac{k}{4(\beta - v_g^2)}|B|^2 B = 0 \tag{3.2}$$

in the convective one. It follows that an Alfvén plane wave is unstable relatively to both absolute or convective longitudinal modulations (an effect that, in the nonlinear regime, leads to longitudinal steepening) when $\beta > v_g^2$ for a right-hand polarization, and $\beta < v_g^2$ for a left-hand polarization. In the limit as $k \to 0$, where $v_g = 1$, we recover the classical stability criteria derived from the one-dimensional DNLS equation (Mjølhus 1976; Spangler *et al.* 1984). Denoting by B_0 the amplitude of the Alfvén-wave train and considering perturbations

https://doi.org/10.1017/S0022377897006119 Published online by Cambridge University Press

proportional to $e^{i(K_x\xi-\Omega\tau)}$, the most-unstable mode for absolute modulation has a wavenumber

$$(K_x)_{\max}=\left[\frac{kv_g}{2(\beta-v_g^2)\,\omega''}\right]^{1/2}B_0 \tag{3.3}$$

and a (temporal) growth rate

$$\Im(\Omega)_{\max}=\frac{kv_g}{4|v_g^2-\beta|}B_0^2. \tag{3.4}$$

In the convective regime, the most-unstable mode has a frequency

$$\Omega_{\max}=\left[\frac{kv_g^3}{2(\beta-v_g^2)\,\omega''}\right]^{1/2}B_0 \tag{3.5}$$

and a (spatial) growth rate

$$\Im(K_x)_{\max}=\frac{|k|}{4|v_g^2-\beta|}B_0^2. \tag{3.6}$$

Note that the neighbourhood of the resonance $\beta=v_g^2$, where the modulation analysis breaks down, should be avoided. Furthermore as stressed by Spangler (1989) and Medvedev and Diamond (1995), when β is of order unity or larger, the above conclusions can be significantly affected by kinetic effects, which extend the instability range of left-hand polarized waves to any β.

3.2. Transverse or static modulational instability

The opposite limit is associated to perturbations that are purely transverse ($\partial_\xi=0$) for absolute modulation or purely static ($\partial_\tau=0$) for the convective one. In the former case,

$$\delta=0,\qquad \bar{u}_x=\frac{1}{v_g}|B|^2,\qquad \bar{b}_x=-\frac{k^2}{2(\beta+1)\,\omega^2}|B|^2,$$

while in the latter,

$$\delta=\frac{1}{2}\left(\frac{1}{\beta}+\frac{k^2+\omega^2}{\omega^2}\right)|B|^2,\qquad \bar{u}_x=0,\qquad \bar{b}_x=-\frac{k^2+\omega^2}{2\omega^2}|B|^2.$$

For transverse absolute modulation, the dynamics is thus governed by

$$i\partial_\tau B+\alpha\Delta_\perp B-kv_g\left[\frac{1}{v_g^2}-\frac{k^4}{4(\beta+1)\,\omega^4}\right]|B|^2B=0, \tag{3.7}$$

while for static convective modulation, it obeys

$$i\partial_\xi B+\frac{\alpha}{v_g}\Delta_\perp B+\frac{k}{4}\left[\frac{1}{\beta}+\frac{(k^2+\omega^2)^2}{\omega^4}\right]|B|^2B=0. \tag{3.8}$$

It follows that left-hand polarized Alfvén-wave trains are unstable to absolute modulation when $\beta>\omega^2/k^2$, and to convective modulation when $\beta<\omega^2/k^2$, in agreement with numerical observations of Kuo *et al.* (1988*b*). For right-hand polarization, the absolute instability range corresponds to

$$\omega^2/k^2<\beta<\omega^4/[k^2(\omega^2-k^2)],$$

https://doi.org/10.1017/S0022377897006119 Published online by Cambridge University Press

and the convective one to $\beta < \omega^2/k^2$ or $\beta > \omega^4/[k^2(\omega^2-k^2)]$ (the latter quantity always being larger than 4). In the nonlinear regime, both instabilities lead to the collapse of Alfvén-wave packets.

Denoting by B_0 the amplitude of the Alfvén-wave train and considering transverse perturbations proportional to $e^{i(\mathbf{K}_\perp\cdot\mathbf{r}-\Omega\tau)}$ (absolute modulation), the most-unstable mode is associated with a transverse wavenumber

$$(K_\perp)_{\max} = \left\{-\frac{kv_g}{\alpha}\left[\frac{1}{v_g^2}-\frac{k^4}{4(\beta+1)\,\omega^4}\right]\right\}^{1/2} B_0, \tag{3.9}$$

with a (temporal) growth rate

$$\Im(\Omega)_{\max} = k\left[\frac{1}{v_g}-\frac{v_g\,k^4}{4(\beta+1)\,\omega^4}\right]B_0^2. \tag{3.10}$$

For static perturbations (convective modulation) proportional to $e^{i(\mathbf{K}_\perp\cdot\mathbf{r}+K_x\xi)}$, the most-unstable mode is associated with

$$(K_\perp)_{\max} = \left\{\frac{kv_g}{4\alpha}\left[\frac{1}{\beta}+\frac{(k^2+\omega^2)^2}{\omega^4}\right]\right\}^{1/2} B_0, \tag{3.11}$$

and its (spatial) growth rate is

$$\Im(K_x)_{\max} = \frac{k}{4}\left[\frac{1}{\beta}+\frac{(k^2+\omega^2)^2}{\omega^4}\right]B_0^2, \tag{3.12}$$

reproducing, in the case of long waves and cold plasmas, the analysis of Shukla and Stenflo (1989) (who used a different definition of the parameter β). Note that in the convective regime, both the growth rate and the transverse wavenumber of the most-unstable mode diverge in the limit as $\beta \to 0$, making stationary convective instabilities impossible in the cold-plasma limit.

3.3. Filamentation-dominated regime

For small values of β, the right-hand polarized wave is only subject to transverse focusing, while the left-hand polarized wave undergoes both longitudinal steepening (provided that $\beta < v_g^2$) and convective filamentation. It is therefore of interest to compare in the latter case the typical distances $l_{\rm phys} = \epsilon\, 2\pi/\Im(K_x)$, or, in a rescaled form, $l = kl_{\rm phys}(\delta B)^2$, associated with the two effects, where δB and k are the amplitude and wavenumber of the carrying Alfvén wave.

Figure 2 shows, for different values of the carrier wavenumber ($k/R_i \to 0$, $k/R_i = 0.1$, 0.6 and 1), the variation with β of the typical length l associated with longitudinal and transverse focusing of left-hand polarized waves. It is noticeable that, for small enough β, the filamentation requires a distance significantly shorter than the longitudinal steepening when k/R_i is small. As an example for $k/R_i = 0.1$, this ratio is about 8×10^{-2} when $\beta = 0.1$. Furthermore, as also obtained in Shukla and Stenflo (1989), the filamentation distance tends to zero with β, suggesting the restriction of the above conclusion to the range $\beta \gg \epsilon$, or, in other words, to values of β larger than the relative level of the magnetic fluctuation intensity, in order to keep the transverse scale of the most-unstable mode (which scales like $\beta^{1/2}$) larger than the carrying Alfvén wavelength.

https://doi.org/10.1017/S0022377897006119 Published online by Cambridge University Press

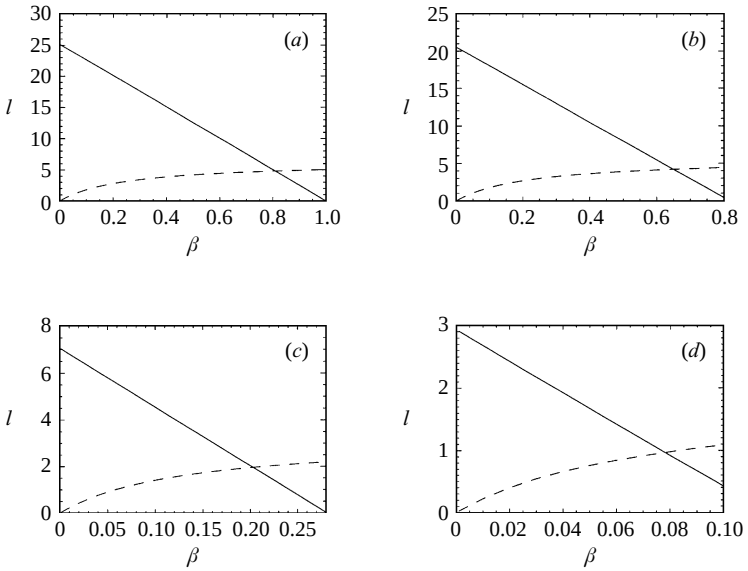


Figure 2. Variation with β of the minimal length for longitudinal steepening (solid line) and for filamentation (dashed line) of left-hand polarized Alfvén waves, for different values of the carrier wavenumber: (*a*) $k/R_i \to 0$; (*b*) $k/R_i = 0.1$; (*c*) 0.6; (*d*) 1.0.

4. Deviations from purely transverse or static modulations

The possible dominant character of the filamentation pointed out in the previous section suggests that we investigate the effect of small deviations from the idealized cases of purely transverse (absolute) or stationary (convective) modulations. This is conveniently done by performing additional rescalings.

(i) In the absolute regime, we write $\tilde{\xi} = \mu\xi$ with $\mu \ll 1$. Equation (2.33) then reduces to

$$\bar{b}_x = -\frac{\beta}{\beta+1}\delta - \frac{k^2}{2(\beta+1)\omega^2}|B|^2. \tag{4.1}$$

Furthermore, the longitudinal and temporal dispersions are negligible in (2.30). Defining the parameter $\eta = \epsilon^{1/2}\mu^{-1}$, we obtain (after dropping the tildes)

$$i\partial_\tau B + \alpha\Delta_\perp B + kv_g\left\{-\frac{1}{v_g}\bar{u}_x + \frac{1}{2}\left[1 + \frac{\beta k^2}{(\beta+1)\omega^2}\right]\delta + \frac{k^4}{4(\beta+1)\omega^4}|B|^2\right\}B = 0, \tag{4.2}$$

$$\eta\partial_\tau\delta - v_g\partial_\xi\delta + \partial_\xi\bar{u}_x = 0, \tag{4.3}$$

$$\eta\partial_\tau\bar{u}_x - v_g\partial_\xi\bar{u}_x + \partial_\xi\left\{\frac{\beta}{\beta+1}\delta + \frac{1}{2}\left[1 - \frac{\beta k^2}{(\beta+1)\omega^2}\right]|B|^2\right\} = -i\eta\frac{\alpha}{v_g}(B\Delta_\perp B^* - B^*\Delta_\perp B). \tag{4.4}$$

https://doi.org/10.1017/S0022377897006119 Published online by Cambridge University Press

(ii) In the convective regime, we define $\tilde{\tau} = \mu\tau$ with $\mu \ll 1$ and again write $\eta = \epsilon^{1/2}\mu^{-1}$. In this case, (2.30)–(2.33) reduce (after dropping the tildes) to

$$i\partial_\xi B + \frac{\alpha}{v_g}\Delta_\perp B + k\left\{-\frac{1}{v_g}\bar{u}_x + \frac{1}{2}\left[1+\frac{\beta k^2}{(\beta+1)\,\omega^2}\right]\delta + \frac{k^4}{4(\beta+1)\,\omega^4}|B|^2\right\}B = 0, \tag{4.5}$$

$$\eta\partial_\xi \bar{u}_x - \frac{1}{v_g}\partial_\tau \bar{u}_x + \partial_\tau \delta = 0, \tag{4.6}$$

$$\left(\eta\partial_\xi - \frac{1}{v_g}\partial_\tau\right)\left\{\frac{\beta}{\beta+1}\delta + \frac{1}{2}\left[1-\frac{\beta k^2}{(\beta+1)\,\omega^2}\right]|B|^2\right\} + \partial_\tau \bar{u}_x = -i\eta\frac{\alpha}{v_g}(B\Delta_\perp B^* - B^*\Delta_\perp B). \tag{4.7}$$

The purely transverse absolute or steady convective regimes studied in Sec. 3 correspond to the limit $\eta \to \infty$. Here we concentrate on finite values of η. The limit $\eta \to 0$, associated with an 'adiabatic dynamics' of the acoustic waves, is exactly solvable. It leads in both cases to a nonlinear Schrödinger equation with a potential

$$V = \frac{k}{4}\left\{\frac{k^4}{(\beta+1)\,\omega^4} - \frac{\beta+1}{(\beta+1)\,v_g^2-\beta}\left[1-\frac{\beta k^2}{(\beta+1)\,\omega^2}\right]^2\right\}|B|^2, \tag{4.8}$$

which vanishes in the long-wavelength limit $k \to 0$. For finite k, it is easily seen that both left- and right-hand polarized Alfvén waves are modulationally stable as long as $\beta < \omega^2/k^2$ and k/R_i is taken smaller than a value close to 0.45.

A richer dynamics is obtained for η of order unity. Linearizing (4.2)–(4.4) and (4.5)–(4.7) around a wave train of amplitude B_0, and considering perturbations proportional to $e^{i(\mathbf{K}\cdot\mathbf{r}-\Omega\tau)}$ with $\mathbf{K} = (K_x, \mathbf{K}_\perp)$ and $K_\perp = |\mathbf{K}_\perp|$, the dispersion relation is as follows:

(i) in the absolute regime,

$$\begin{aligned}
&-\eta^2\Omega^4 - 2\eta v_g K_x \Omega^3 \\
&+\left\{\left(\frac{\beta}{\beta+1} - v_g^2\right)K_x^2 + \eta^2\alpha^2 K_\perp^4 + \eta^2\frac{\alpha k}{v_g}B_0^2 K_\perp^2\left[2 - \frac{k^4 v_g^2}{2(\beta+1)\,\omega^4}\right]\right\}\Omega^2 \\
&+\eta\left\{2\alpha^2 v_g K_x K_\perp^4 + \alpha k B_0^2 K_x K_\perp^2\left[2 - \frac{k^4 v_g^2 + 2\beta k^2\omega^2}{(\beta+1)\,\omega^4}\right]\right\}\Omega \\
&+\alpha k v_g B_0^2\left[\frac{k^4(\beta - v_g^2) - 2\beta k^2\omega^2}{2(\beta+1)\,\omega^4} + \frac{1}{2}\right]K_x^2 K_\perp^2 \\
&+\alpha^2\left(v_g^2 - \frac{\beta}{\beta+1}\right)K_x^2 K_\perp^4 = 0;
\end{aligned} \tag{4.9}$$

https://doi.org/10.1017/S0022377897006119 Published online by Cambridge University Press

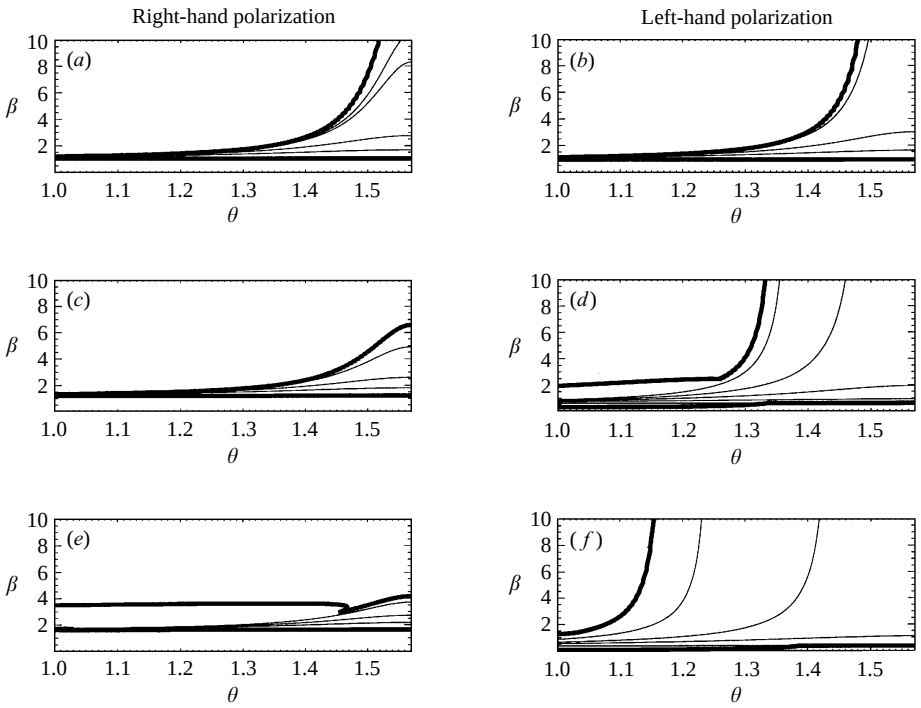


Figure 3. Growth-rate contours (rescaled by $|\mathbf{K}|$) in the ($\theta = \arctan(K_\perp/K_x)$, β) plane, of the most-unstable right- and left-hand polarized Alfvén waves, relative to quasitransverse absolute modulation, for $\eta = \sqrt{0.1}$ and different values of k/R_i: (*a*, *b*) $k/R_i = 0.05$; (*c*) 0.20; (*d*) 0.50; (*e*) 0.70; (*f*) 1.00. The thick lines limits the instability domain. Note that for right-hand polarization, the value of k/R_i cannot exceed $1/\sqrt{2}$.

(ii) in the convective regime,

$$\eta^2\beta v_g^2 K_x^4 + 2\eta\beta v_g \Omega K_x^3$$
$$+\left\{[\beta-(\beta+1)\,v_g^2]\,\Omega^2-\eta^2\alpha^2\beta K_\perp^4+\tfrac{1}{2}\eta^2\alpha k v_g B_0^2\left[1+\beta\frac{(k^2+\omega^2)^2}{\omega^4}\right]K_\perp^2\right\}K_x^2$$
$$+\eta\left[\alpha k B_0^2\left(\frac{\beta k^4}{\omega^4}-\beta-1\right)\Omega K_\perp^2-2\frac{\alpha^2\beta}{v_g}\Omega K_\perp^4\right]K_x$$
$$+\frac{\alpha k}{2v_g}B_0^2\left[\beta+1-2\frac{\beta k^2}{\omega^2}+\frac{k^4}{\omega^4}(\beta-v_g^2)\right]K_\perp^2\,\Omega^2$$
$$+\alpha^2\left(\beta+1-\frac{\beta}{v_g^2}\right)K_\perp^4\,\Omega^2=0. \tag{4.10}$$

Figure 3 displays, in the case of the absolute instability, for both right- and left-hand polarizations, the contours of the growth rate $\Im(\Omega)$ (rescaled by $|\mathbf{K}|$) of the most-unstable mode in the plane ($\beta, \theta = \arctan(K_\perp/K_x)$), with $K_x \ll K_\perp$, for $|\mathbf{K}| = 0.01$, $\eta = \sqrt{0.1}$ and different values of k/R_i, preserving the condition $k \gg |\mathbf{K}|$. Similarly, Fig. 4 displays, in the case of the convective instability, the contours of the growth rate $\Im(K_x)$ (rescaled by $|\mathbf{K}_\perp|$) of the most-unstable mode

https://doi.org/10.1017/S0022377897006119 Published online by Cambridge University Press

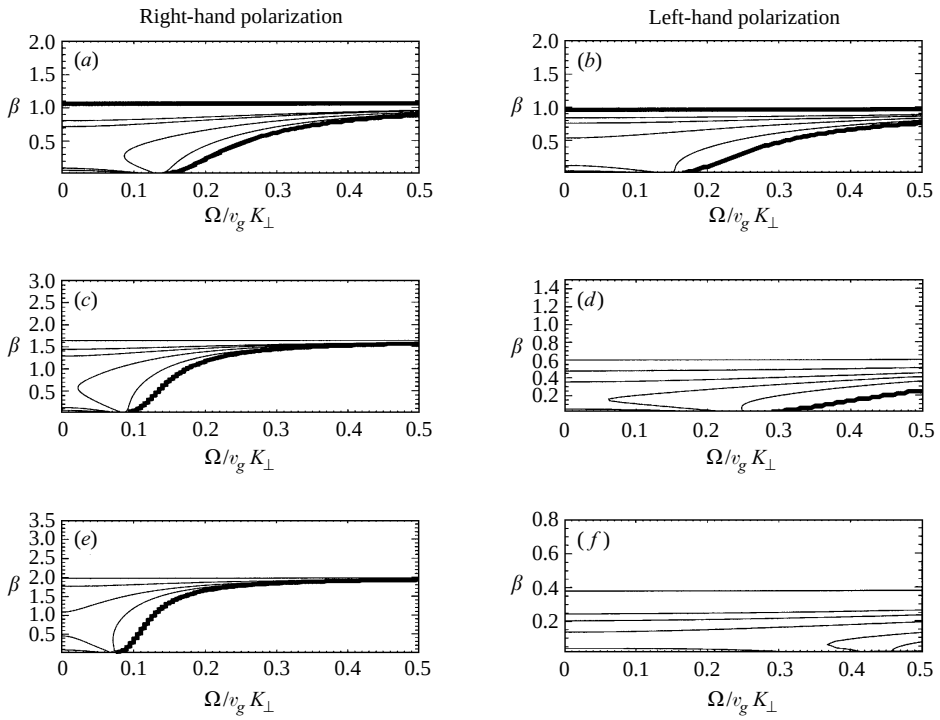


Figure 4. Growth-rate contours (rescaled by $|\mathbf{K}_\perp|$) in the $(\Omega/(v_g K_\perp), \beta)$ plane, of the most unstable right- and left-hand polarized Alfvén waves, relative to quasitransverse convective modulation, for $\eta = \sqrt{0.1}$ and different values of k/R_i: (*a*, *b*) $k/R_i = 0.05$; (*c*, *d*) 0.50; (*e*) 0.70; (*f*) 1.00. The thick lines limit the instability domain. Note that for right-hand polarization the value of k/R_i cannot exceed $1/\sqrt{2}$.

in the $(\beta, \Omega/(K_\perp v_g))$ plane, with $\Omega \ll K_\perp$, for $K_\perp = 0.01$, $\eta = \sqrt{0.1}$ and different values of k/R_i satisfying $k \gg K_\perp$. For both the absolute and convective regimes, the neighbourhood of the resonance $\beta = \omega^2/k^2$ should be ignored, since the asymptotics breaks down in this region. For right- and left-hand polarized Alfvén waves, the absolute modulational instability, which occurs when $\beta > \omega^2/k^2$ for purely transverse perturbations, extends into an unstable region near $\theta = \frac{1}{2}\pi$. Similarly, the convective instability leads, when $\beta < \omega^2/k^2$, to an unstable range near $\Omega = 0$ (and also, when k is taken large enough, to a weakly unstable region for $\beta > \omega^2/k^2$, not visible in Fig. 4). Note that, in the case of left-hand polarized waves, the range of instability increases with the value of k/R_i, in both the convective and absolute regimes. In contrast, for right-hand polarized waves, in the convective regime, this range shrinks to a limit domain as k/R_i increases (Fig. 4), while in the absolute one, the range of values of β for the instability to occur (away from the resonance) is reduced as k/R_i increases to its limit value $1/\sqrt{2}$ prescribed by the condition $\omega < R_i$ (Fig. 3).

5. Nonlinear dynamics

The modulation equations (4.2)–(4.4) and (4.5)–(4.7) are convenient for a linear stability analysis. In the nonlinear regime, a more usual form is obtained by performing the transformation discussed at the end of Sec. 2 and the change of

https://doi.org/10.1017/S0022377897006119 Published online by Cambridge University Press

variables introduced at the beginning of Sec. 4. In the absolute case, the ponderomotive force becomes $(\eta/v_g)\,\partial_\tau|B|^2$, and we are led to define $v_x = \bar{u}_x - |B|^2/v_g$ while in the convective one, the ponderomotive force takes the form $\eta\partial_\xi|B|^2$ and we write

$$d = \frac{\delta}{\beta+1} - \frac{1}{2}\left[\frac{1}{\beta} + \frac{k^2}{(\beta+1)\,\omega^2}\right]|B|^2.$$

We obtain the following results:

(i) for the absolute regime,

$$i\partial_\tau B + \alpha\Delta_\perp B + kv_g\left\{-\frac{1}{v_g}v_x + \frac{1}{2}\left[1+\frac{\beta k^2}{(\beta+1)\,\omega^2}\right]\delta + \left[-\frac{1}{v_g^2} + \frac{k^4}{4(\beta+1)\,\omega^4}\right]|B|^2\right\}B = 0, \quad (5.1)$$

$$\eta\partial_\tau\delta - v_g\,\partial_\xi\delta + \partial_\xi v_x + \frac{1}{v_g}\partial_\xi|B|^2 = 0, \quad (5.2)$$

$$\eta\partial_\tau v_x - v_g\,\partial_\xi v_x + \frac{\beta}{\beta+1}\partial_\xi\delta - \frac{1}{2}\left[1+\frac{\beta k^2}{(\beta+1)\,\omega^2}\right]\partial_\xi|B|^2 = 0, \quad (5.3)$$

(ii) for the convective regime,

$$i\partial_\xi B + \frac{\alpha}{v_g}\Delta_\perp B + k\left\{-\frac{1}{v_g}\bar{u}_x + \frac{\beta+1}{2}\left[1+\frac{\beta k^2}{(\beta+1)\,\omega^2}\right]d + \frac{1}{4}\left[\frac{1}{\beta} + \frac{(k^2+\omega^2)^2}{\omega^4}\right]|B|^2\right\}B = 0, \quad (5.4)$$

$$\eta\partial_\xi d - \frac{1}{v_g}\partial_\xi d + \frac{1}{\beta}\partial_\tau\bar{u}_x - \frac{1}{v_g\beta}\partial_\tau|B|^2 = 0, \quad (5.5)$$

$$\eta\partial_\xi\bar{u}_x - \frac{1}{v_g}\partial_\tau\bar{u}_x + (\beta+1)\,\partial_\tau d + \frac{\beta+1}{2\beta}\left[1+\frac{\beta k^2}{(\beta+1)\,\omega^2}\right]\partial_\tau|B|^2 = 0. \quad (5.6)$$

Equations (5.1)–(5.3) can be viewed as Zakharov–Rubenchik-type equations (Zakharov and Rubenchik 1972; Zakharov and Schulman 1991) describing the coupling of a high-frequency wave to low-frequency acoustic-type waves. In the present case, however, the acoustic-wave equations include only longitudinal derivatives, because, to leading order, the transverse velocity is slaved to the transverse magnetic field (see (2.19)).

5.1. Quasitransverse absolute modulation

We rescale as follows:

$$\tilde{\xi} = |k|\,\xi, \qquad \tilde{\tau} = |k|\,|v_g|\,\tau, \qquad \tilde{Y} = \left(\frac{|kv_g|}{|\alpha|}\right)^{1/2} Y, \qquad \tilde{Z} = \left(\frac{|kv_g|}{|\alpha|}\right)^{1/2} Z, \quad (5.7)$$

$$|B|^2 = \frac{|\tilde{B}|^2}{Q_1}, \qquad v_x = -\frac{A_1}{|v_g|\,Q_1}\tilde{v}_x, \qquad \delta = -\frac{A_1}{Q_1\,v_g^2}\tilde{\delta}, \quad (5.8)$$

https://doi.org/10.1017/S0022377897006119 Published online by Cambridge University Press

where

$$A_1 = \frac{1}{2}\left[1+\frac{\beta k^2}{(\beta+1)\,\omega^2}\right], \qquad Q_1 = \frac{1}{v_g^2}\left[1-\frac{k^2\omega^2}{(\beta+1)\,(k^2+\omega^2)^2}\right].$$

Dropping the tildes, (5.1)–(5.3) become

$$i\partial_\tau B = -\sigma_1\,\Delta_\perp B + \sigma_2[W_1(\delta + D_1\,v_x) + |B|^2]\,B, \tag{5.9}$$

$$\eta\partial_\tau\delta - \sigma_3\,\partial_\xi\delta = -\partial_\xi v_x - D_1\,\partial_\xi|B|^2, \tag{5.10}$$

$$\eta\partial_\tau v_x - \sigma_3\,\partial_\xi v_x = -\frac{1}{M_1^2}\,\partial_\xi\delta - \partial_\xi|B|^2, \tag{5.11}$$

where

$$M_1 = |v_g|\left(\frac{\beta+1}{\beta}\right)^{1/2}, \qquad D_1 = -\frac{\sigma_3}{A_1}, \qquad W_1 = \frac{A_1^2}{v_g^2\,Q_1}.$$

Furthermore, $\sigma_1 = \mathrm{sign}(\alpha)$, $\sigma_2 = \mathrm{sign}(kv_g)$ and $\sigma_3 = \mathrm{sign}(v_g)$.

5.2. Quasistatic convective modulation

We rescale ξ, τ, Y and Z as in (5.7), and take

$$|B|^2 = \frac{|\tilde{B}|^2}{Q^2}, \qquad \bar{u}_x = \frac{A_2\,|v_g|}{Q_2}\tilde{u}_x, \qquad d = \frac{A_2\,v_g^2}{\beta Q_2}\tilde{d}, \tag{5.12}$$

with

$$A_2 = \frac{\beta+1}{2\beta}\left[1+\frac{\beta k^2}{(\beta+1)\,\omega^2}\right], \qquad Q_2 = \frac{1}{4}\left[\frac{1}{\beta}+\left(\frac{k^2+\omega^2}{\omega^2}\right)^2\right].$$

Dropping the tildes, (5.4)–(5.6) become

$$i\partial_\xi B = -\sigma_1\,\sigma_3\,\Delta_\perp B - \sigma_2\,\sigma_3[W_2(d + D_2\,u_x) + |B|^2]\,B, \tag{5.13}$$

$$\eta\partial_\xi d - \sigma_3\,\partial_\tau d = -\partial_\tau u_x - D_2\,\partial_\tau|B|^2, \tag{5.14}$$

$$\eta\partial_\xi u_x - \sigma_3\,\partial_\tau u_x = -\frac{1}{M_2^2}\,\partial_\tau d - \partial_\tau|B|^2, \tag{5.15}$$

where

$$M_2 = \frac{1}{|v_g|}\left(\frac{\beta}{\beta+1}\right)^{1/2}, \qquad D_2 = -\frac{\sigma_3}{|v_g|^2\,A_2}, \qquad W_2 = \frac{|v_g|^2\,A_2^2}{Q_2}.$$

The variation with k/R_i of the coefficients in (5.9)–(5.11) and (5.13)–(5.15) is illustrated in Figs 5 and 6 respectively, for the two polarizations, when $\beta = 1.5$ and $\beta = 0.5$.

5.3. A unified formulation

The equations governing the absolute and the convective dynamics can be rewritten in unified form as

$$i\partial_t B = -\sigma\Delta_\perp B + \sigma'[W(d + Du) + |B|^2]\,B, \tag{5.16}$$

$$\eta\partial_t d - \sigma_3\,\partial_x d = -\partial_x u - D\partial_x|B|^2, \tag{5.17}$$

$$\eta\partial_t u - \sigma_3\,\partial_x u = -\frac{1}{M^2}\,\partial_x d - \partial_x|B|^2, \tag{5.18}$$

https://doi.org/10.1017/S0022377897006119 Published online by Cambridge University Press

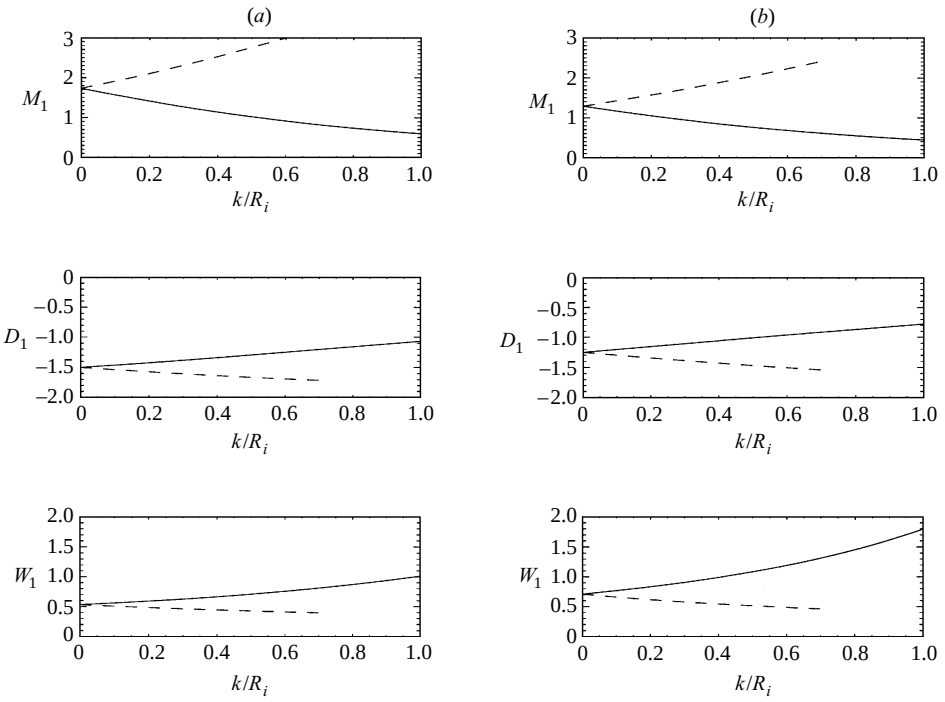


Figure 5. Variation with k/R_i of the coefficients M_1, D_1 and W_1 appearing in (5.9)–(5.11) for absolute modulation when $\beta = 0.5$ (*a*) and 1.5 (*b*). Solid and dashed lines refer to left- and right-hand polarizations respectively.

where the variable t refers either to time or to the distance from the source (in the latter case x refers to time). The coefficients in (5.16)–(5.18) are specified by identification with the absolute or the convective systems (5.9)–(5.11) or (5.13)–(5.15).

The system (5.16)–(5.18) for the acoustic waves is diagonalized by introducing the Riemann invariants ($j = 1, 2$)

$$Z_j = \frac{W}{2}\left[1 + (-1)^j \frac{D}{M}\right][d + (-1)^j Mu], \tag{5.19}$$

which obey

$$\eta \partial_t Z_j + \Lambda_j \partial_x Z_j = (-1)^{j+1} \frac{W(M + (-1)^j D)^2}{2M} \partial_x |B|^2, \tag{5.20}$$

with

$$\Lambda_j = -\sigma_3 + (-1)^j \frac{1}{M}.$$

The equation for the Alfvén-wave amplitude then becomes

$$i\partial_t B = -\sigma \Delta_\perp B + \sigma'(|B|^2 + Z_1 + Z_2) B. \tag{5.21}$$

A resonance associated to the vanishing of the eigenvalue Λ_2 is a priori possible in the considered range $k > 0$ and $\omega > 0$. It corresponds to $M = 1$, which requires $v_g < 1$ in both the absolute and convective regimes. As can be

https://doi.org/10.1017/S0022377897006119 Published online by Cambridge University Press

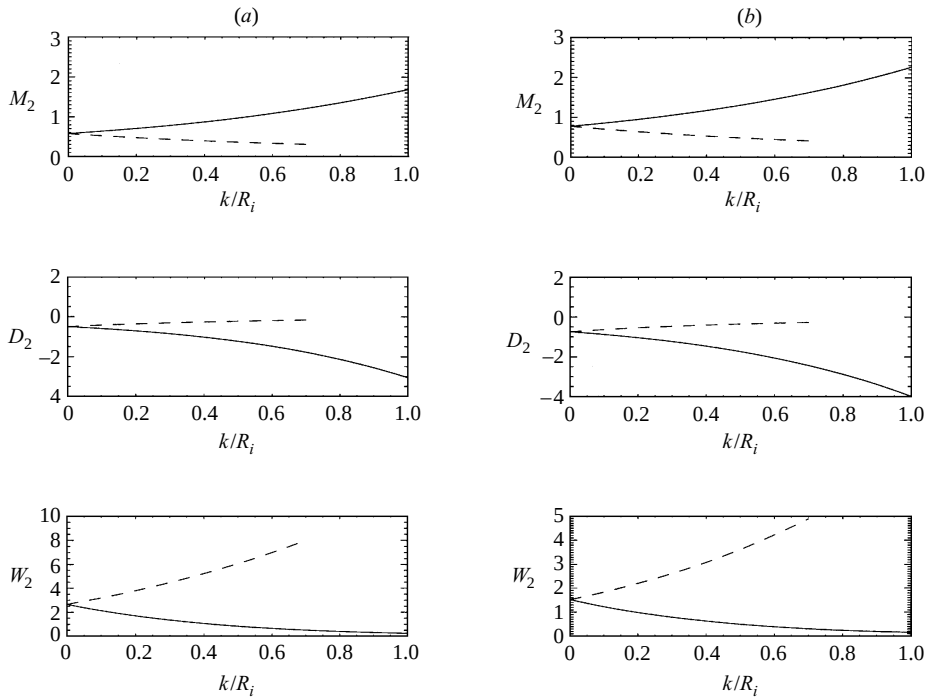


Figure 6. Variation with k/R_i of the coefficients M_2, D_2 and W_2 appearing in (5.13)–(5.15) for convective modulation when $\beta = 0.5$ (a) and $\beta = 1.5$ (b). Solid and dashed lines refer to left- and right-hand polarizations respectively.

seen in Fig. 1(b), this is only possible with a left-hand polarized wave. Nevertheless, the ponderomotive force stirring the resonant wave Z_2 is weak – smaller by a factor of $r = [(1+D)/(1-D)]^2$ than the ponderomotive force acting on the non-resonant wave Z_1. For example, in the convective regime, assuming $\beta = 0.5$, the resonant wavenumber is $k \approx 0.53$, leading to $D \approx -1.3$ and $r \approx 1.7 \times 10^{-2}$, thus making the resonance irrelevant.

Equations (5.20) and (5.21) were studied in Sec. 2 of Passot *et al.* (1996).† Integrating along the characteristics $x_j(a,t) = \lambda_j t + a$, with $\lambda_j = \Lambda_j/\eta$, we get

$$Z_j(\mathbf{r}, x_j(a,t), t) = Z_j(\mathbf{r}, a, 0) + (-1)^{j+1}\frac{WM}{2\eta}\left[1+(-1)^j\frac{D}{M}\right]^2\int_0^t |B|_x^2(\mathbf{r}, x_j(a,\tau),\tau)\,d\tau, \quad (5.22)$$

where $\mathbf{r}$ is the transverse vector coordinate. At early times, the acoustic waves Z_1 and Z_2 are negligible in (5.21), where the variable x then reduces to a parameter. Assuming that $\sigma\sigma' < 0$, the carrying wave first focuses in the transverse planes for which the initial L^2 norm $|B_0(.,x)|_{L^2(\mathbb{R}^2)}$ exceeds the critical value for collapse (Weinstein 1986). Since the rate of collapse in these planes depends on $|B_0(.,x)|_{L^2(\mathbb{R}^2)}$, strong gradients then develop along the x direction,

† In this reference, this system appears as the limit of the Zakharov–Rubenchik equations in the case where modulation is quasilongitudinal (in order to make the transverse Laplacian negligible in the equations for the acoustic waves) and the dispersion subdominant. Note that in the case of Alfvén waves, these transverse derivatives are absent, and a finite dispersion at the scale of the carrying wave can be retained.

https://doi.org/10.1017/S0022377897006119 Published online by Cambridge University Press

producing a significant ponderomotive force. The latter stirs acoustic waves, which in turn can react back on the focusing process. The analysis of this dynamics presented in Passot *et al.* (1996) is based on the ansatz that, as long as the carrying wave is not qualitatively affected by the acoustic waves, its amplitude near collapse keeps the form

$$|B(\mathbf{r},x,t)| = a(x) f(t_*(x-x_c(t))-t)\, R(b(x) f(t_*(x-x_c(t))-t)\,\mathbf{r}), \tag{5.23}$$

where $x_c(t)$ is the focus location and $t_*(x)$ can be viewed as an x-dependent singularity time. The functions $a(x)$ and $b(x)$ are smooth rescaling coefficients, while f denotes the blowing factor. Two regimes can then be distinguished, according to the speed of the magnetosonic wave and the distance t_*-t from the singularity time: at fixed t_*-t, for rapidly propagating magnetosonic waves ($\eta \ll 1$), the adiabatic regime is obtained in the form

$$Z_j(\mathbf{r},x_j(t),t) = (-1)^{j+1}\frac{MW}{2\Lambda_j}\left[1+(-1)^j\frac{D}{M}\right]^2 |B|^2. \tag{5.24}$$

In the opposite case, at a fixed velocity of the magnetosonic waves (not necessarily small), the limit as $t_*-t\to 0$ leads to

$$Z_j(\mathbf{r},x,t) \approx (-1)^j\frac{WM}{2\eta}\left[1+(-1)^j\frac{D}{M}\right]^2 t'_*(x)\,|B|^2(\mathbf{r},x,t). \tag{5.25}$$

Equation (5.25) indicates that, sufficiently close to the singularity, the adiabatic approximation becomes invalid and a transition takes place where the Z_j become antisymmetric with respect to the centre of the collapsing pulse, the function $t'_*(z)$ itself being antisymmetric.

If the collapse is not arrested during this adiabatic phase, the developing antisymmetric profiles of Z_1 and Z_2 will affect the potential in such a way that the focus will be shifted in the x direction on the side where the waves reinforce the potential. The resulting dynamics deserves a numerical investigation. In contrast with the situation addressed in Passot *et al.* (1996), where the parameter η was kept equal to unity (and the initial conditions fixed) and the collapse was never arrested, the possibility we have here of varying the length or duration of the initial pulse permits different evolutions.

5.3.1. Numerical simulations. Numerical integrations of (5.16)–(5.18) were performed for axisymmetric solutions using the anisotropic dynamical rescaling method introduced in Landman *et al.* (1991) and presented in the appendix of Passot *et al.* (1996).

A resolution of 200 grid points was used in both the longitudinal and radial directions. As initial conditions, we considered a localized wave packet $B = 4e^{-(x^2+r^2)}$ with $d = u = 0$, which corresponds to

$$u_x = 0, \qquad \rho = \frac{|B|^2}{2\beta}$$

for the convective case and to

$$u_x = \frac{|B|^2}{v_g}, \qquad \rho = -\frac{k^2}{2\omega^2(\beta+1)}|B|^2$$

https://doi.org/10.1017/S0022377897006119 Published online by Cambridge University Press

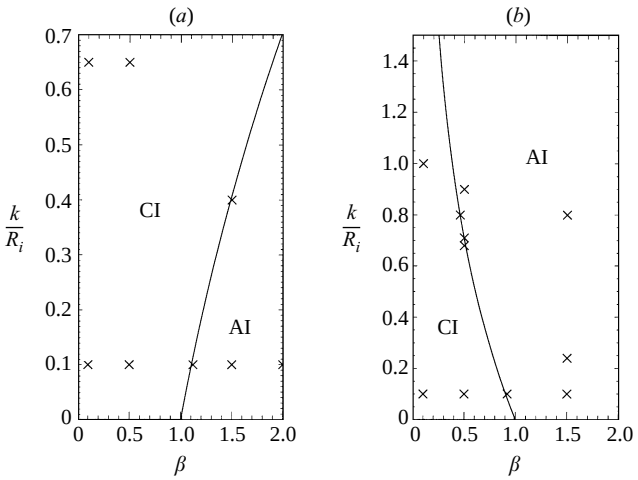


Figure 7. Resonant curve $\beta = \omega^2/k^2$ separating the ranges of convective (CI) and absolute (AI) modulational instabilities for right-hand (a) and left-hand (b) polarized Alfvén waves. The crosses indicate the different values of β and k used in the numerical simulations of Sec. 5.

for the absolute one. The values of β and k retained in our simulations are indicated by crosses on Fig. 7, which also display, for each polarization, the regions of the $(\beta, k/R_i)$ plane associated with absolute and convective instabilities and separated by the curve $\beta = \omega^2/k^2$. Note that for small β, the convective instability occurs for both polarizations, at small enough k, while, at sufficiently large k, only left-hand polarized waves are absolutely unstable (Fig. 7). The parameter η, which measures the length (for absolute modulation) or the duration (for convective modulation) of the initial Alfvén-wave packet, was taken equal to 0.1, 0.3, 0.4 and 1. For both the absolute and convective instabilities, regardless of the Alfvén-wave polarization and whatever the values of β and of the carrying wavenumber, three different regimes are encountered, according to the value of the parameter η: adiabatic arrest of the filamentation for $\eta = 0.1$, arrest of the filamentation with formation of acoustic fronts for $\eta = 0.3$ or 0.4, and collapse for $\eta = 1$.

Typical results of the simulations are presented in Figs 8–10, which, in the convective case, display at various points on the axis $r = 0$ the temporal variation of the Alfvén-wave envelope $|B|$ and of the magnetosonic waves d and u.

In Figure 8, which corresponds to $\eta = 0.1$, $k/R_i = 0.1$, $\beta = 0.5$ and left-hand polarization, the filamentation is rapidly inhibited under the effect of the developing magnetosonic waves. These waves first display an antisymmetric profile whose left part is, for small η, rapidly advected away from the Alfvén-wave packet. The other part stays beneath the pulse, and reaches its adiabatic limit, producing a caviton that in the small-k limit, cancels out the nonlinearity in the equation for the Alfvén-wave envelope.

In Fig. 9, where $\eta = 0.3$ with $k/R_i = 1$, $\beta = 0.1$ and left-hand polarization, the focusing of the Alfvén-wave packet is arrested. In this case, however, the magnetosonic waves develop underneath the Alfvén pulse a sharp anti-symmetric acoustic front, whose strength increases with η as a consequence of

https://doi.org/10.1017/S0022377897006119 Published online by Cambridge University Press

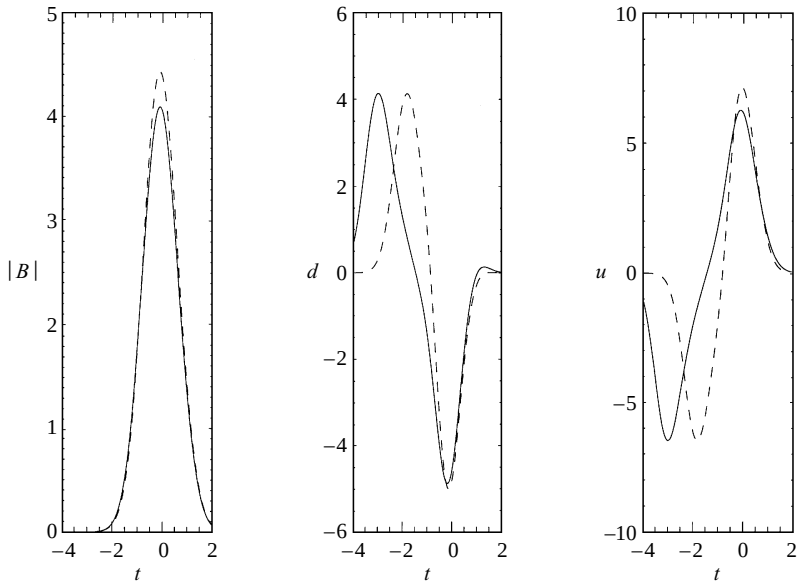


Figure 8. Arrest of convective filamentation with adiabatic dynamics of the magnetosonic waves, for $\eta = 0.1$, $k/R_i = 0.1$, $\beta = 0.5$ and left-hand polarization. The time evolutions of $|B|$, d and u_x are shown on the $r = 0$ axis, at the points $x = 0.0734$ (dashed line) and $x = 0.119$ (solid line) respectively behind and beyond the location of the filamentation arrest.

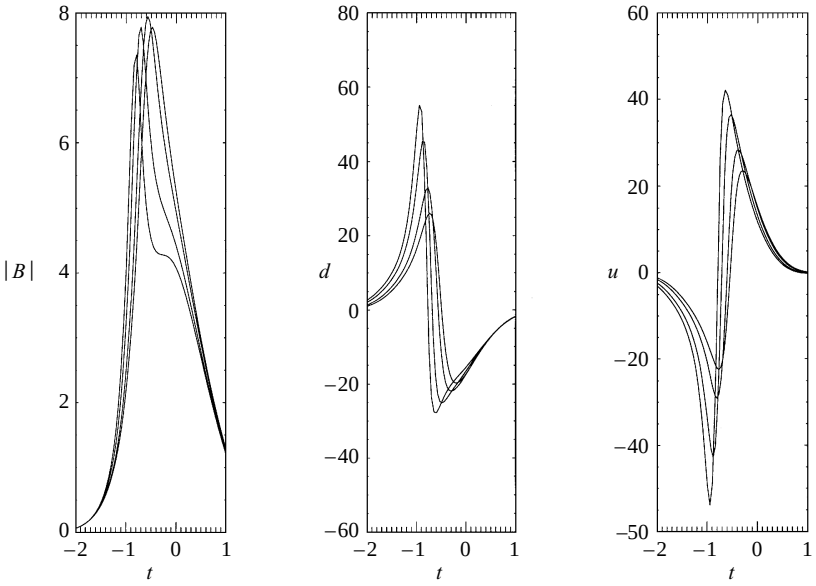


Figure 9. Arrest of filamentation with formation of strong acoustic fronts for $\eta = 0.3$, $k/R_i = 1$, $\beta = 0.1$ and left-hand polarization. The time evolutions of $|B|$, d and u_x are shown on the $r = 0$ axis, at the point $x = 0.139$ behind the filamentation arrest and at the points $x = 0.149$, $x = 0.166$, $x = 0.177$ beyond it.

https://doi.org/10.1017/S0022377897006119 Published online by Cambridge University Press

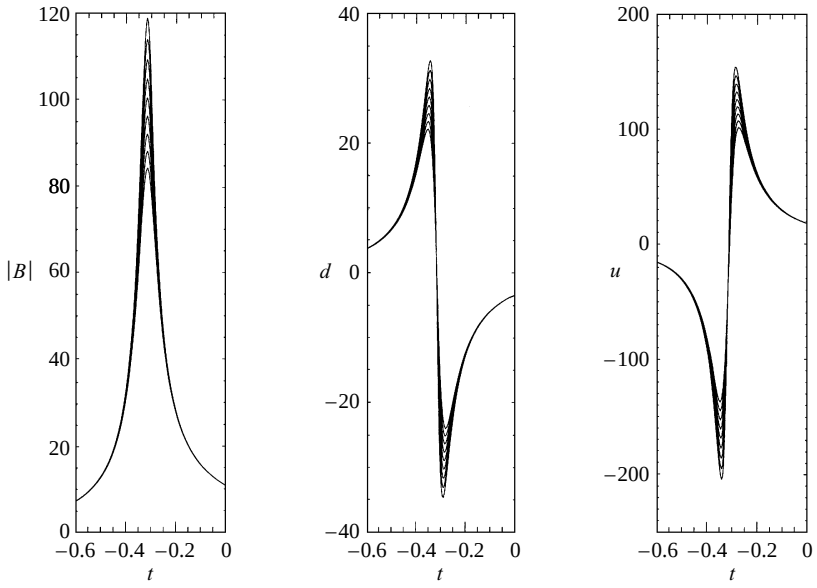


Figure 10. Finite-distance wave collapse for $\eta = 1$, $k/R_i = 0.65$, $\beta = 0.5$ and right-hand polarization. The time evolutions of $|B|$, d and u_x are shown at various points on the $r = 0$ axis, located between $x = 0.156$ and $x = 0.16$, near the collapse.

the amplification of the potential in the nonlinear Schrödinger equation. This leads to strong hydrodynamic effects not included in the envelope formalism, which only retains a linear description of the hydrodynamic phenomena.

Finally, in Fig. 10, where $\eta = 1$ with $k/R_i = 0.65$, $\beta = 0.5$ and right-hand polarization, the filamentation is not arrested. A sharp antisymmetric magnetosonic front develops, and the Alfvén wave collapses at a finite distance.

This indicates that the three different behaviours obtained by Passot *et al.* (1994) for the absolute dynamics in the small-k limit with large enough β are not restricted to this regime, but provide a general description of Alfvén-wave filamentation.

6. Conclusions

The main conclusion of this paper is that when the phase velocity of an Alfvén-wave train exceeds the sound speed, it undergoes a convective-type filamentation instability, which may dominate the longitudinal steepening. In the nonlinear regime, the development of this instability leads to three different scenarios, according to the duration of the initial pulse. When the latter is very long ($\eta \gg 1$), Alfvén-wave packets can collapse in a finite distance, leading to the so-called filamentation process. The local blow-up of the wave amplitude is then only limited by small-scale phenomena not included in the present analysis. When the duration of the initial pulse is redued ($\eta = O(1)$), the development of large-scale mangetosonic waves can arrest this amplification, leading to the formation of intense acoustic fronts and strong hydrodynamic effects. Finally, for very short pulses ($\eta \ll 1$), the magnetosonic waves adiabatically follow the Alfvén-wave intensity. They renormalize, and in the

https://doi.org/10.1017/S0022377897006119 Published online by Cambridge University Press

long-wavelength limit even cancel the potential of the nonlinear Schrödinger equation governing the Alfvén-wave packet, leading to defocusing.

Alfvén-wave filamentation has recently been considered as a possible heating mechanism in the solar corona and the warm ionized phase of the interstellar medium (Champeaux *et al*. 1997). A still-debated question indeed concerns the acceleration of the fast solar wind that originates from open coronal holes (a quiet region of the solar atmosphere). Two mechanisms are usually proposed. The first refers to the standard dissipation processes that take place at the base of the corona, where the wave amplitude is small ($\delta B/B \ll 1$). It requires the presence of small scales, possibly resulting from the inhomogeneities of the plasma. The second mechanism is the turbulent dissipation that occurs at large distances from the Sun, where $\delta B/B \approx 1$. Both processes in fact appear to be insufficient to explain the observed velocities of the solar wind (see e.g. Leer *et al*. 1982; Esser *et al*. 1986; Hollweg 1992; Narain and Ulmschneider 1996). A first quantitative estimate of the energy dissipation resulting from convective Alfvén-wave filamentation shows that, even in the time-independent limit where no shock waves form, this process plays a significant role in the solar corona.

Acknowledgements

We thank S. Spangler for useful discussions. The numerical calculations were performed on the CRAY C94 and C98 of the Institut du Développement et des Ressources Informatiques Scientifiques, Orsay. This work benefited from partial support of the Human Capital and Mobility European cooperative network 'Numerical Simulations of Nonlinear Magnetohydrodynamic Phenomena' (ERBC HRXCT930410).

Appendix

At $O(\epsilon)$, the equations for the transverse fields are

$$\partial_t u_1 - \partial_x b_1 = -\partial_T u_{1/2} + \partial_X b_{1/2}, \tag{A 1}$$

$$\partial_t b_1 - \partial_x u_1 + \zeta \frac{i}{R_i} \partial_{xx} b_1 = -\partial_T b_{1/2} + \partial_X u_{1/2} - \zeta \frac{2i}{R_i} \partial_{Xx} b_{1/2}. \tag{A 2}$$

The solvability condition is

$$k(-\partial_T U_{1/2} + \partial_X B_{1/2}) - \omega\left(-\partial_T B_{1/2} + \partial_X U_{1/2} + \partial_X U_{1/2} + \zeta \frac{2k}{R_i} \partial_X B_{1/2}\right) = 0, \tag{A 3}$$

or

$$\partial_T B_{1/2} + v_g \partial_X B_{1/2} = 0, \tag{A 4}$$

with a group velocity $v_g = 2\omega^3/[k(k^2+\omega^2)]$. Equations (A 1) and (A 2) are then solved in the form

$$\begin{pmatrix} b_1 \\ u_1 \end{pmatrix} = \left[\begin{pmatrix} 1 \\ \dfrac{-k}{\omega} \end{pmatrix} B_1 + \begin{pmatrix} 0 \\ \dfrac{i}{\omega}\left(\partial_X + \dfrac{k}{\omega}\partial_T\right) B_{1/2} \end{pmatrix} \right] e^{i(kx-\omega t)}, \tag{A 5}$$

https://doi.org/10.1017/S0022377897006119 Published online by Cambridge University Press

where the B_1 term refers to a null-space element that corrects the leading order of the wave amplitude.

At $O(\epsilon^{3/2})$, we have

$$\begin{aligned}\partial_t u_{3/2}-\partial_x b_{3/2} = &-\partial_T u_1+\partial_X b_1-\partial_\perp(\beta\rho_1+b_{x1})\\ &-\rho_1\partial_t u_{1/2}-u_{x1}\partial_x u_{1/2}+b_{x1}\partial_x b_{1/2}+\tfrac{1}{2}\zeta b_{1/2}(\partial_\perp^* b_{1/2}-\partial_\perp b_{1/2}^*)\\ &-\tfrac{1}{2}(u_{1/2}^*\partial_\perp+u_{1/2}\partial_\perp^*)u_{1/2},\end{aligned} \tag{A 6}$$

$$\begin{aligned}\partial_t b_{3/2}-\partial_x u_{3/2}+\zeta\frac{i}{R_i}\partial_{xx}b_{3/2} = &-\partial_T b_1+\partial_X u_1-\zeta\frac{i}{R_i}\partial_{XX}b_{1/2}\\ &+\partial_x(u_{1/2}b_{x1}-u_{x1}b_{1/2})+\tfrac{1}{2}\zeta i\partial_\perp(u_{1/2}b_{1/2}^*-u_{1/2}^*b_{1/2})\\ &+\zeta\frac{i}{R_i}\partial_x[\rho_1\partial_x b_{1/2}-b_{x1}\partial_x b_{1/2}+\partial_\perp(b_{x1}-\tfrac{1}{2}|b_{1/2}|^2)]\\ &-\zeta\frac{i}{R_i}\partial_x[\tfrac{1}{2}b_{1/2}(\partial_\perp^* b_{1/2}-\partial_\perp b_{1/2}^*)+2\partial_X b_1],\end{aligned} \tag{A 7}$$

$$\partial_t\rho_{3/2}+\partial_x u_{x3/2} = -\partial_T\rho_1-\partial_X u_{x1}-\tfrac{1}{2}(\partial_\perp^* u_1+\partial_\perp u_1^*), \tag{A 8}$$

$$\partial_t u_{x3/2}+\beta\partial_x\rho_{3/2} = -\partial_T u_{x1}-\beta\partial_X\rho_1-\tfrac{1}{2}\partial_X|b_{1/2}|^2-\tfrac{1}{2}\partial_x(b_1^*b_{1/2}+b_1b_{1/2}^*), \tag{A 9}$$

$$\partial_x b_{x3/2} = -\partial_X b_{x1}-\tfrac{1}{2}(\partial_\perp^* b_1+\partial_\perp b_1^*), \tag{A 10}$$

$$\begin{aligned}\partial_t b_{x3/2} = &-\partial_T b_{x1}-\tfrac{1}{2}(\partial_\perp^* u_1+\partial_\perp u_1^*)+\zeta\frac{i}{2R_i}\partial_X(\partial_\perp^* b_{1/2}-\partial_\perp b_{1/2}^*)\\ &+\zeta\frac{i}{2R_i}\partial_x(\partial_\perp^* b_1-\partial_\perp b_1^*).\end{aligned} \tag{A 11}$$

The solvability condition that eliminates the resonant oscillating modes on the right-hand sides of (A 6) and (A 7) is

$$\begin{aligned}i(\partial_T B_1+v_g\partial_X B_1)-\frac{\omega}{k^2+\omega^2}\left(-\frac{\omega^2}{k^2}\partial_{XX}-\frac{k^2}{\omega^2}\partial_{TT}-\frac{2k}{\omega}\partial_{XT}\right)B_{1/2}\\ +\alpha\Delta_\perp B_{1/2}-kv_g\left(\frac{1}{v_g}\bar{u}_{x1}+\frac{k^2}{2\omega^2}\bar{b}_{x1}-\frac{1}{2}\delta_1\right)B_{1/2}=0.\end{aligned} \tag{A 12}$$

where

$$\delta_1=\bar{\rho}_1-\bar{b}_{x1},\qquad \alpha=\frac{k\omega}{k^2+\omega^2}\left[\frac{\omega^2}{2k^3}-\frac{\beta k}{2(\beta k^2-\omega^2)}\right].$$

Combining (A 4) and (A 12), we obtain for $B=B_{1/2}+\epsilon^{1/2}B_1$ the Schrödinger-type equation

$$\begin{aligned}i(\partial_T B+v_g\partial_X B)-\epsilon^{1/2}\frac{\omega}{k^2+\omega^2}\left(-\frac{\omega^2}{k^2}\partial_{XX}-\frac{k^2}{\omega^2}\partial_{TT}-\frac{2k}{\omega}\partial_{XT}\right)B\\ +\epsilon^{1/2}\alpha\Delta_\perp B+\epsilon^{1/2}kv_g\left(-\frac{1}{v_g}\bar{u}_{x1}-\frac{k^2}{2\omega^2}\bar{b}_{x1}+\frac{1}{2}\delta_1\right)B=0,\end{aligned} \tag{A 13}$$

https://doi.org/10.1017/S0022377897006119 Published online by Cambridge University Press

where we have used the leading order of (A 13) to estimate the $\epsilon^{1/2}$ longitudinal and temporal dispersive terms that arise in the $\epsilon^{1/2}$ correction term.

Elimination of the non-oscillating secular terms in (A 6)–(A 11) leads to

$$\partial_T \bar{u}_1 - \partial_X \bar{b}_1 + \partial_\perp \left[\beta\delta_1 + (\beta+1)\,\bar{b}_{x1} + \frac{k^2}{2\omega^2}|B_{1/2}|^2 \right] = 0, \tag{A 14}$$

$$\partial_T \bar{b}_1 - \partial_X \bar{u}_1 = 0, \tag{A 15}$$

$$\partial_T \delta_1 + \partial_X \bar{u}_{x1} = 0, \tag{A 16}$$

$$\partial_T \bar{u}_{x1} + \beta\partial_X(\delta_1 + \bar{b}_{x1}) + \tfrac{1}{2}\partial_X|B_{1/2}|^2 = 0, \tag{A 17}$$

$$\partial_X \bar{b}_{x1} + \tfrac{1}{2}(\partial_\perp^* \bar{b}_1 + \partial_\perp \bar{b}_1^*) = 0, \tag{A 18}$$

$$\partial_T \bar{b}_{x1} + \tfrac{1}{2}(\partial_\perp^* \bar{u}_1 + \partial_\perp \bar{u}_1^*) = 0. \tag{A 19}$$

Combining (A 18), (A 19) and (A 14), we obtain

$$\partial_{TT} \bar{b}_{x1} - \partial_{XX} \bar{b}_{x1} - \Delta_\perp \left[\beta\delta_1 + (\beta+1)\,\bar{b}_{x1} + \frac{k^2}{2\omega^2}|B_{1/2}|^2 \right] = 0. \tag{A 20}$$

Equations (A 13), (A 20), (A 16) and (A 17) constitute a closed system from which reference to $\bar{b}_1$ and $\bar{u}_1$ has been eliminated. However, the last two equations display a degeneracy when the modulation is purely transverse, and higher-order terms are to be retained in a spectral 'angular boundary layer' associated with quasitransverse perturbations. We are thus led to consider at order ϵ^2 the equations

$$\begin{aligned} \partial_t \rho_2 + \partial_x u_{x2} = {} & -\partial_\tau \rho_{3/2} - \partial_x(\rho_1 u_{x1}) - \partial_X u_{x3/2} \\ & - \tfrac{1}{2}(\partial_\perp^* u_{3/2} + \partial_\perp u_{3/2}^*) - \tfrac{1}{2}[\partial_\perp^*(\rho_1 u_{1/2}) + \partial_\perp(\rho_1 u_{1/2}^*], \end{aligned} \tag{A 21}$$

$$\begin{aligned} \partial_t u_{x2} + \beta\partial_x \rho_2 = {} & -\partial_\tau u_{x3/2} - \rho_1 \partial_t u_{x1} - \beta\partial_X \rho_{3/2} \\ & - \tfrac{1}{2}\partial_x[u_{x1}^2 + \beta(\gamma-1)\,\rho_1^2 + 2|b_1|^2] \\ & - \tfrac{1}{2}(u_{1/2}^* \partial_\perp + u_{1/2}\partial_\perp^*)\,u_{x1} + \tfrac{1}{2}(b_{1/2}^* \partial_\perp + b_{1/2}\partial_\perp^*)\,b_{x1} \\ & - \tfrac{1}{2}\partial_x(b_{1/2} b_{3/2}^* + b_{1/2}^* b_{3/2}) - \tfrac{1}{2}\partial_X(b_{1/2} b_1^* + b_{1/2}^* b_1), \end{aligned} \tag{A 22}$$

$$\begin{aligned} \partial_t b_{x2} = {} & -\partial_\tau b_{x3/2} + \tfrac{1}{2}[\partial_\perp^*(u_{x1} b_{1/2}) + \partial_\perp(u_{x1} b_{1/2})^*] \\ & - \tfrac{1}{2}[\partial_\perp^*(u_{1/2} b_{x1}) + \partial_\perp(u_{1/2} b_{x1})^*] - \tfrac{1}{2}(\partial_\perp^* u_{3/2} + \partial_\perp u_{3/2}^*) \\ & - \zeta \frac{1}{2iR_i}[\partial_X(\partial_\perp^* b_1 - \partial_\perp b_1^*) + \partial_x(\partial_\perp^* b_{3/2} - \partial_\perp b_{3/2}^*)] \\ & - \zeta \frac{1}{2iR_i}\{\partial_\perp^*[(b_{x1} - \rho_1)\,\partial_x b_{1/2}] - \partial_\perp[(b_{x1} - \rho_1)\,\partial_x b_{1/2}]^*\} \\ & - \zeta \frac{1}{4iR_i}(\partial_\perp^* b_{1/2} + \partial_\perp b_{1/2}^*)\,(\partial_\perp^* b_{1/2} - \partial_\perp b_{1/2}^*) \\ & - \zeta \frac{1}{4iR_i}(b_{1/2}\partial_\perp^* + b_{1/2}^* \partial_\perp)\,(\partial_\perp^* b_{1/2} - \partial_\perp b_{1/2}^*). \end{aligned} \tag{A 23}$$

https://doi.org/10.1017/S0022377897006119 Published online by Cambridge University Press

The solvability conditions corresponding to the elimination of the non-oscillating secular terms are

$$\partial_T \bar{\rho}_{3/2} + \partial_X \bar{u}_{x3/2} = -\tfrac{1}{2}(\partial_\perp^* \bar{u}_{3/2} + \partial_\perp \bar{u}_{3/2}^*) - \tfrac{1}{2}[\partial_\perp^*(\tilde{\rho}_1^* U_{1/2}) + \partial_\perp(\tilde{\rho}_1 U_{1/2}^*)], \quad \text{((A 24)}$$

$$\partial_T \bar{u}_{x3/2} + \beta\partial_X \bar{\rho}_{3/2} = i\omega(\tilde{\rho}_1^* \tilde{u}_{x1} - \tilde{\rho}_1 \tilde{u}_{x1}^*) - \tfrac{1}{2}(U_{1/2}^* \partial_\perp \tilde{u}_{x1} + U_{1/2} \partial_\perp^* \tilde{u}_{x1}^*)$$
$$+ \tfrac{1}{2}(B_{1/2}^* \partial_\perp \tilde{b}_{x1} + B_{1/2} \partial_\perp^* \tilde{b}_{x1}^*) - \tfrac{1}{2}\partial_X(B_{1/2} B_1^* + B_{1/2}^* B_1), \quad \text{(A 25)}$$

$$\partial_T \bar{b}_{x3/2} = -\tfrac{1}{2}(\partial_\perp^* \bar{u}_{3/2} + \partial_\perp \bar{u}_{3/2}^*)$$
$$- \tfrac{1}{2}[\partial_\perp^*(\tilde{b}_{x1}^* U_{1/2} - \tilde{u}_{x1}^* B_{1/2}) + \partial_\perp(\tilde{b}_{x1} U_{1/2}^* - \tilde{u}_{x1} B_{1/2}^*)]$$
$$- \zeta \frac{k}{2R_i}\{\partial_\perp^*[(\tilde{b}_{x1} - \tilde{\rho}_1)^* B_{1/2}] + \partial_\perp[(\tilde{b}_{x1} - \tilde{\rho}_1) B_{1/2}^*]\}$$
$$- \zeta \frac{i}{4R_i}(B_{1/2} \Delta_\perp B_{1/2}^* - B_{1/2}^* \Delta_\perp B_{1/2})$$
$$+ \zeta \frac{i}{2R_i} \partial_X(\partial_\perp^* \bar{b}_1 - \partial_\perp \bar{b}_1^*). \quad \text{(A 26)}$$

Using (2.15), (2.16), (2.19) and (2.27)–(2.29), the equation satisfied by $\delta_{3/2} = \bar{\rho}_{3/2} - \bar{b}_{x3/2}$ reduces to

$$\partial_T \delta_{3/2} + \partial_X \bar{u}_{x3/2} = -\zeta \frac{i}{2R_i} \partial_X(\partial_\perp^* \bar{b}_1 - \partial_\perp \bar{b}_1^*), \quad \text{(A 27)}$$

while (A 25) can be rewritten as

$$\partial_T \bar{u}_{x3/2} + \beta\partial_X(\delta_{3/2} + \bar{b}_{x3/2})$$
$$= i\lambda(B_{1/2} \Delta_\perp B_{1/2}^* - B_{1/2}^* \Delta_\perp B_{1/2}) - \tfrac{1}{2}\partial_X(B_{1/2}^* B_1 + B_{1/2} B_1^*), \quad \text{(A 28)}$$

with

$$\lambda = \frac{1}{4}\left[\frac{\beta k^3}{\omega^2(\beta k^2 - \omega^2)} - \frac{1}{k}\right] = -\frac{\alpha}{v_g}.$$

Combining (A 16) and (A 27), (A 17) and (A 28) for the mean longitudinal fields, we find that $\delta = \delta_1 + \epsilon^{1/2}\delta_{3/2}$, $\bar{u}_x = \bar{u}_{x1} + \epsilon^{1/2}\bar{u}_{x3/2}$ and $\bar{b}_x = \bar{b}_{x1} + \epsilon^{1/2}\bar{b}_{x3/2}$ obey

$$\partial_T \delta + \partial_X \bar{u}_x = 0, \quad \text{(A 29)}$$

$$\partial_T \bar{u}_x + \beta\partial_X(\delta + \bar{b}_x) + \tfrac{1}{2}\partial_X|B|^2 = i\lambda\epsilon^{1/2}(B\Delta_\perp B^* - B^*\Delta_\perp B), \quad \text{(A 30)}$$

where the term $-[i\epsilon^{1/2}/(2R_i)]\,\partial_X(\partial_\perp^* \bar{b} - \partial_\perp \bar{b}^*)$ has been neglected in (A 29), since it is always smaller than $\partial_X \bar{u}_x$. In contrast, in (A 30), the ordering can be broken in the case of quasitransverse perturbations, for which the longitudinal derivative can become comparable to the corrective term $i\lambda\epsilon^{1/2}(B\Delta_\perp B^* - B^*\Delta_\perp B)$. Also, owing to the absence of degeneracy, it is enough to retain for $\bar{b}_x$ the leading order and drop the subscript indices in (A 20). This leads to (2.30)–(2.33) of Sec. 2.

References

Belcher, J. W. and Davis, L. 1971 Large-amplitude Alfvén waves in the interplanetary medium, 2. *J. Geophys. Res.* **76**, 3534–3563.

https://doi.org/10.1017/S0022377897006119 Published online by Cambridge University Press

Belcher, J. W., Davis, L. and Smith, E. J. 1969 Large-amplitude Alfvén waves in the interplanetary medium: Mariner 5. *J. Geophys. Res.* **76**, 2302–2308.

Champeaux, S., Gazol, A., Passot, T. and Sulem, P. L. 1997 Plasma heating by Alfvén wave filamentation: a relevant mechanism in the solar corona and the interstellar medium. *Astrophys. J.* **486**, Sept. (in press).

Esser, R., Leer, E., Habbal, S. R. and Withbroe, G. L. 1986 A two-fluid solar wind model with Alfvén waves: parameter study and application to observations. *J. Geophys. Res.* **91**, 2950–2960.

Galinsky, V. L., Schevchenko, V. I., Medvedev, M. V. and Diamond, P. H. 1996 Emergence of dissipative structures in coherent nonlinear Alfvén waves. Preprint.

Hada, T. 1993 Evolution of large amplitude Alfvén waves in the solar wind with $\beta \sim 1$. *Geophys. Res. Lett.* **20**, 2415–2418.

Hollweg, J. V. 1992 Status of solar wind modeling from the transition region outwards. *Solar Wind Seven* (ed. E. Marsch and R. Schwenn), pp. 53–60. Pergamon Press, Oxford.

Hoshino, M. 1988 Evolution of nonlinear polarization in localised and finite amplitude Alfvén waves. *Phys. Fluids* **33**, 3271–3279.

Kuo, S. P. P., Wang, M. H. and Lee, M. C. 1988*a* Filamentation instability of large-amplitude Alfvén waves. *J. Geophys. Res.* **93**, 9621–9627.

Kuo, S. P. P., Wang, M. H. and Schmidt, G. 1988*b* Convective filamentation instability of circularly polarized Alfvén waves. *Phys. Fluids* **B4**, 734–740.

Landman, M., Papanicolaou, G., Sulem, C., Sulem, P. L. and Wang, X. P. 1991 Stability of isotropic singularities for the nonlinear Schrödinger equation. *Physica* **D47**, 393–415.

Leer, E., Holzer, T. E. and Flå, T. 1982 Acceleration of the solar wind. *Space Sci. Rev.* **33**, 161–200.

Medvedev, M. V. and Diamond, P. H. 1995 Fluid models for kinetic effects on coherent nonlinear Alfvén waves. I. Fundamental theory. *Phys. Plasmas* **3**, 863–873.

Medvedev, M. V. and Diamond, P. H. 1996 On the theory of quasiparallel Alfvén wave dynamics with collisionless dissipation and noise. Preprint.

Mio, K., Ogino, T., Minami, K. and Takeda, S. 1975 Modified nonlinear Schrödinger equation for Alfvén waves propagating along the magnetic field in cold plasmas. *J. Phys. Soc. Japan* **41**, 265–271.

Mjølhus, E. 1976 On the modulational instability of hydromagnetic waves parallel to the magnetic field. *J. Plasma Phys.* **16**, 321–334.

Mjølhus, E. and Wyller, J. 1986 Alfvén solitons. *Physica Scripta* **33**, 442–451.

Mjølhus, E. and Wyller, J. 1988 Nonlinear Alfvén waves in a finite-beta plasma. *J. Plasma Phys.* **40**, 299–318.

Mjølhus, E., Flå, T. and Wyller, J. 1989 The effect of resonant particles on Alfvén solitons. *Physica* **D39**, 405–422.

Narain, U. and Ulmschneider, P. 1996 Coronal heating mechanisms II. *Space Sci. Rev.* **75**, 453–509.

Passot, T. and Sulem, P. L. 1993 Multidimensional modulation of Alfvén waves. *Phys. Rev.* **E48**, 2966–2974.

Passot, T. and Sulem, P. L. 1995 Nonlinear dynamics of dispersive Alfvén waves. *Small-Scale Structures in Three-Dimensional Hydrodynamic and Magnetohydrodynamic Turbulence* (ed. M. Meneguzzi, A. Pouquet and P. L. Sulem), pp. 405–410. Lecture Notes in Physics, Vol. 462. Springer-Verlag, Berlin.

Passot, T., Sulem, C. and Sulem, P. L. 1994 Effect of longitudinal modulational on Alfvén wave filamentation. *Phys. Rev.* **E50**, 1427–1436.

Passot, T., Sulem, C. and Sulem, P. L. 1996 Generation of acoustic fronts by focusing wave-packets. *Physica* **D94**, 168–187.

Rogister, A. 1971 Parallel propagation of nonlinear low-frequency waves in high-β plasmas. *Phys. Fluids* **14**, 2733–2739.

Shukla, P. K. and Stenflo, L. 1986 Three-dimensional modulation of electron-cyclotron waves. *Phys. Fluids* **29**, 2479–2483.

https://doi.org/10.1017/S0022377897006119 Published online by Cambridge University Press

Shukla, P. K., Feix, G. and Stenflo, L. 1988 Nonlinearity coupled electromagnetic ion-cyclotron and magnetosonic waves in astrophysical plasmas. *Astrophys. Space Sci.* **147**, 383–388.

Shukla, P. K. and Stenflo, L. 1989 Filamentation instability of Alfvén waves. *Astrophys. Space Sci.* **155**, 145–147.

Stenflo, L. and Shukla, P. K. 1988 Filamentation instability of electron and ion cyclotron waves in the ionosphere. *J. Geophys. Res.* **93**, 4115–4117.

Spangler, S. 1989 Kinetic effects on Alfvén wave nonlinearity II. The modified nonlinear wave equation. *Phys. Fluids* **B2**, 407–418.

Spangler, S., Sheerin, J. P. and Payne, G. L. 1984 A numerical study of nonlinear Alfvén waves and solitons. *Phys. Fluids* **28**, 104–109.

Tu, C. Y. and Marsch, E. 1995 MHD structures, waves and turbulence in the solar wind: observations and theories. *Space Sci. Rev.* **73**, 1–210.

Viñas, A. F. and Goldstein, M. L. 1991*a* Parametric instabilities of circularly polarized large-amplitude dispersive Alfvén waves: excitation of parallel-propagating electromagnetic daughter waves. *J. Plasma Phys.* **46**, 107–127.

Viñas, A. F. and Goldstein, M. L. 1991*b* Parametric instabilities of circularly polarized large-amplitude dispersive Alfvén waves: excitation of obliquely-propagating daughter and side-band waves. *J. Plasma Phys.* **46**, 129–152.

Zakharov, V. E. and Rubenchik, A. M. 1972 Nonlinear interaction between high and low frequency waves. *Prikl. Mat. Tekh. Fiz.* **5**, 84–98.

Zakharov, V. E. and Schulman, E. I. 1991 Integrability of nonlinear systems and perturbation theory. *What is integrability?* (ed. V. E. Zakharov), pp. 185–250. Springer-Verlag, Berlin.

Webb, G. M., Brio, M. and Zank, G. P. 1995 Symmetries of the triple degenerate DNLS equation for weakly nonlinear dispersive MHD waves. *J. Plasma Phys.* **54**, 201–244.

Weinstein, M. I. 1986 On the structure and formation of singularities in solutions to nonlinear dispersive evolution equations. *Commun. Part. Differential Eqns* **11**, 545–565.

https://doi.org/10.1017/S0022377897006119 Published online by Cambridge University Press